Analysis of moisture transport in cementitious materials and modelling of drying-wetting cycles

SSCS 2012
Numerical Modeling
Strategies for Sustainable Concrete Structures
Aix-en-Provence, France
May 29-June 1, 2012

Zhidong Zhang, Mickael Thiéry, Véronique Baroghel-Bouny

Paris-Est University, Paris; Materials Department, IFSTTAR, Paris, France

Abstract

Aiming at studying moisture transport in cementitious materials, the paper describes a multiphase isothermal modelling of moisture transport which incorporates the coupled movements of liquid water, water vapor and dry air. The model is based on mass balance equations, transport laws and material properties, such as water vapor sorption properties and permeability. Numerical simulations show that a gas overpressure can occur owing to the evaporation coupled with the diffusion of dry air while a gas underpressure is observed if the initial saturation is close to saturated state. The moisture transport during drying is either in liquid form or vapor form depending on external relative humidity and material microstructure (porosity). Furthermore, a simplified method for the modelling of moisture transport during wetting is proposed, using adsorption isotherm and different expressions of relative permeability. Moreover, mass loss kinetics data obtained from experiments during the first drying and wetting cycle are used for the validation of the numerical results.

Keyword: cementitious materials, moisture transport, gas pressure variations, drying-wetting cycles, water vapor sorption isotherm

1. Introduction

In a natural environment, cementitious materials are subjected to cyclic variations of relative humidity (RH), such as from medium level (50%) to water saturation (100%). At the medium level, a decrease in liquid water content engenders strong capillary effects, which may induce shrinkage, tensile stresses, and even cracking if shrinkage is hindered. It is clear that the development of these durability issues mainly depends on the evolution of the liquid water and gaseous phases in cementitious materials. Therefore, a relevant characterization of the durability properties of cementitious materials requires a comprehensive understanding of the drying process and a good reliability in the determination of the moisture transport properties. Daïan [1] proposed a moisture transport process which takes into account vapor diffusion and the discontinuous capillary effects. Bazant et al. [2] use a non-linear diffusion equation to describe the isothermal drying at the macroscopic scale to study the influence of drying on shrinkage of concrete. However, those models are not able to distinguish the contribution of liquid water transport to water vapor diffusion. Philip et al. [3] presented a method supposing drying is a series-parallel process and liquid continuity does not exist. Mainguy et al. [4] have used both experimental and theoretical results to reveal the gas pressure variation and pointed out that a gas overpressure appears in the cementitious materials based on a multiphase model. Thiery et al [5] also got similar results by analysing moisture transport properties.

On the contrary, if the material is submitted to high RH, water vapor diffuses from the surrounding environment to the inner part of the material, according to wetting process, which may lead to swelling effects and thus may also reduce the durability. Because of hysteresis, wetting does not correspond to a reversible process of drying. Therefore a different method is needed to model wetting. Various approaches have been used to simulate moisture transport with a possible distinction between drying and wetting according to sorption isotherms [6, 7] or by using different diffusion coefficients [7].

Based on previous works [5], this paper constitutes a further development to analyse isothermal drying properties (such as properties related to gas pressure variations or to moisture transport modes). Then we introduce a simple method for the modelling of wetting, considering hysteresis between desorption and adsorption. Experimental data were obtained on three OPC pastes CN, CO and CP [8] (cylindrical specimens with 7 cm diameter and 14 cm height). The main characteristics of these materials (W/C and accessible-to-water porosity ϕ measured by hydrostatic weighting after vacuum saturation followed by a drying at 105°C at the age of 200-day sealed curing) are gathered in Table 1.

Table 1. Material characteristics

Materials	W/C	ϕ (%)
CO	0.35	0.30
CN	0.45	0.45
CP	0.60	0.58

2. Modelling of isothermal drying

2.1. Mass balance equations

At the macroscopic scale of an elementary representative volume, drying of cementitious materials can be described continuously in time and space by a set of partial differential equations which are mass balance equations for liquid water (l), water vapor (v) and dry air (a):

$$\frac{\partial[\rho_l \phi S_l]}{\partial t} = -\mathrm{div}\, w_l - \mu \tag{1}$$

$$\frac{\partial[\rho_v \phi (1 - S_l)]}{\partial t} = -\mathrm{div}\, w_v + \mu \tag{2}$$

$$\frac{\partial[\rho_a \phi (1 - S_l)]}{\partial t} = -\mathrm{div}\, w_a \tag{3}$$

where ρ_i is the mass density of each component i (=l, v or a) and S_l is the liquid water saturation. μ denotes the rate of liquid water mass changing into vapor per unit volume of porous material and w_i is the flux of component i.

2.2. Transport laws

The flux of liquid water is expressed by the generalized Darcy's law for unsaturated conditions, which reads:

$$w_l = -\rho_l \frac{K}{\eta_l} k_{rl}(S_l) \mathbf{grad}\, p_l \tag{4}$$

In this equation, K is the intrinsic permeability of the porous material. p_l stands for the liquid water pressure. η_l and $k_{rl}(S_l)$ are the dynamic viscosity of liquid water and the relative permeability, respectively.

The movement of water vapor and dry air are both governed by advection of the gaseous mixture and by molecular diffusion. The advection of the gaseous mixture can be described by Darcy's law in the same way as liquid water. The diffusion of moisture in the form of water vapor is driven by a gradient of molar fraction according to Fick's first law. The expressions of water vapor and dry air fluxes are given as (where $i = v$ or a):

$$w_i = -\rho_i \frac{K}{\eta_g} k_{rg}(S_l) \mathbf{grad}\, p_g - \frac{M_i p_{atm}}{RT} f(\phi, S_l) D_{va}\, \mathbf{grad} \left(\frac{p_i}{p_g}\right) \tag{5}$$

where $k_{rg}(S_l)$ and η_g represent the relative permeability and the dynamic viscosity of the gaseous phase, respectively. R is the ideal gas constant, T is the absolute temperature, M_i is the molar mass of component i, $f(\phi, S)$ is the resistance factor for gas diffusion, D_{va} is the free water vapor diffusion coefficient in the air (2.47×10^{-5} m^2·s^{-1} at T = 293 ± 1 K) [9].

Among the various empirical expressions for $f(\phi, S_l)$, the one proposed by Millington [10], originally developed for granular materials, has been applied by several authors [4-5, 9] for partially saturated porous media such as cementitious materials:

$$f(\phi, S_l) = \phi^a (1 - S_l)^b \tag{6}$$

where a and b are two parameters related to the morphology of the microstructure. Mainguy et al. [4] used a = 4/3 and b = 10/3, which leads up to an overestimation of the vapor diffusion compared

with the proposal of a = 2.74 and b = 4.20 by Thiery et al. [5] from the fitting of experimental data obtained by Papadakis et al. [11] (see Fig. 1). The values proposed by Thiery et al. are chosen in the present research since they seem more relevant for cementitious materials. The comparison of resistance factor for CO, CN and CP in Fig. 1 shows that CO always has the highest tortuosity effects due to the least porosity.

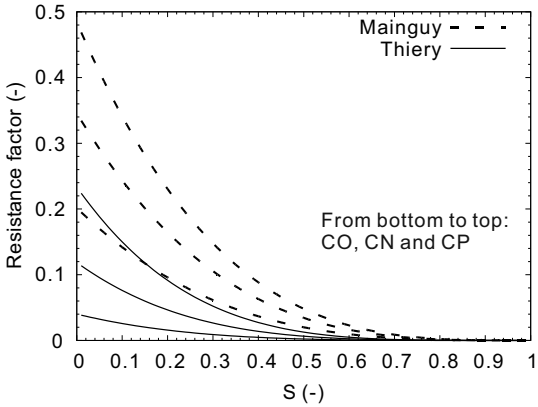

Fig. 1. Resistance factor predicted by Mainguy's choice and Thiery's choice for CO, CN and CP.

2.3. State equations

The gas is assumed as an ideal mixture of water vapor and dry air. Hence, according to Dalton's law, the mixed gas pressure p_g is the sum of pressures of water vapor and dry air ($p_g = p_v + p_a$). The macroscopic capillary pressure (p_c) is defined as the difference between the gas pressure and the liquid water pressure (see Eq. (7)).

$$p_c = p_g - p_l \tag{7}$$

Thermodynamically, it is possible to show that p_c depends on S_l for isothermal conditions [12]. If we assume that liquid water and vapor remain in permanent local thermodynamic equilibrium and the mixture pressure p_g is constantly equal to the atmospheric pressure (p_{atm}), Kelvin's law can be used to link the capillary pressure to RH prevailing inside the pores.

$$p_c = -\frac{\rho_l RT}{M_v}\ln(\mathrm{RH}) \tag{8}$$

2.4. Material properties

2.4.1. Hysteritical properties

The relation $p_c(S_l)$ presents an hysteresis between desorption and adsorption [13] for some materials. In order to express the capillary pressure curve with respect to S_l in a continuous way, a two-parameter analytical function has been proposed by van Genuchten [13].

$$p_c(S_l) = \alpha\left({S_l}^{-\beta} - 1\right)^{1-1/\beta} \tag{9}$$

where parameters α and β are obtained from fitting experimental data. The best fitting parameters for desorption and adsorption isotherms of CO, CN and CP are provided in Table 2 [9]. Associated with Eq. (8), we are able to describe the main adsorption and desorption isotherms with S_l and RH as variables. Sorption isotherms for CO, CN and CP are illustrated in Fig. 2.

Table 2. Fitting parameters used in Eq. (9)

	Parameters	CO	CN	CP
Desorption	α (MPa)	45.35	32.70	13.70
	β (-)	2.12	2.16	2.56
Adsorption	α (MPa)	3.60	1.48	0.73
	β (-)	3.39	3.79	4.01

2.4.2. Intrinsic permeability

The intrinsic permeability K is a key parameter for modelling of moisture transport in cementitious materials. However, the direct measurement of K for low permeability cementitious materials is commonly recognised as very difficult. Indeed, the pressure needed to generate the liquid movement is too high and generally exceeds the compressive strength of the material. Therefore, when no relevant direct method is applicable, an indirect method, proposed by Coussy et al. [14] and widely used in [4, 9, and 15], can be employed to predict K by means of fitting experimental drying kinetics (mass loss *vs*. time) through inverse analysis. Intrinsic permeabilities for CO, CN and CP obtained by the indirect method are presented in Table 3.

Table 3. Intrinsic permeabilities

	CO	CN	CP
K (10^{-20} m^2)	2.7	16.0	605.0

2.4.3. Relative permeability

Relative permeability to liquid water k_{rl} is involved in the generalized Darcy's law (see Eq. (4)). k_{rl} is an increasing function of S_l. A comprehensive numerical model proposed by Mualem [16] to predict the relative permeability of a porous medium from the capillary pressure curves is written as:

$$k_{rl}(S_l) = {S_l}^{1/2}[KL + (1 - KL)KH]^2$$

where

$$KL(S_l) = \left(\int_{p_c}^{+\infty} dL(S_l)/{p_c}^2\right) \Big/ \left(\int_0^{+\infty} dL(S_l)/{p_c}^2\right)$$
$$KH(S_l) = \left(\int_{p_c}^{+\infty} dH(S_l)/{p_c}^2\right) \Big/ \left(\int_0^{+\infty} dH(S_l)/{p_c}^2\right) \quad (10)$$

KL and KH are two normalized integral functions using the capillary pressure as input data. The literature (see [5] and [15]) describes this comprehensive model in more details. Since this equation is based on Mualem's domain theory for desorption [15], it is used for dying in this paper.

Note that one expression of relative permeability to liquid water, derived from van Genuchten [13] and based on Mualem's model [16], has been widely used [4, 7] for modelling of moisture transport in low permeability materials.

$$k_{rl}(S_l) = S_l^{1/2}\left(1 - \left(1 - {S_l}^{\beta}\right)^{1/\beta}\right)^2 \quad (11)$$

where β is the parameter used in Eq. (9). Compared with Eq. (10), the analytical relationship (see Eq. (11)) gives a different prediction of k_{rl} (see Fig. 3). In this paper, we use the analytical relationship for adsorption and values of β are taken from Table 2. The relative permeability to the gaseous phase is expressed as [17]:

$$k_{rg}(S_l) = (1 - S_l)^{1/2}\left(1 - {S_l}^{\beta}\right)^{2/\beta} \quad (12)$$

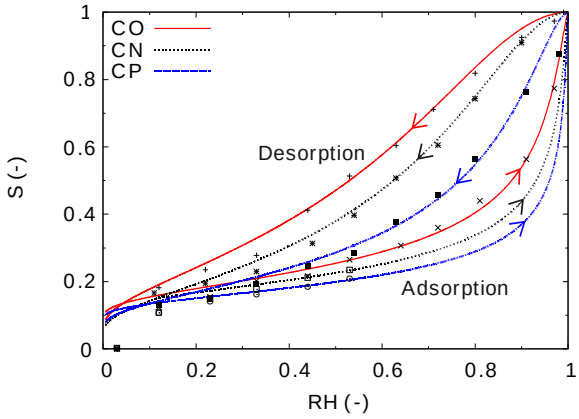

Fig. 2. Desorption and adsorption isotherms of CO, CN and CP. Fitting curves (lines) and experimental data (symbols) [8, 15]. The hysteretic loops are illustrated.

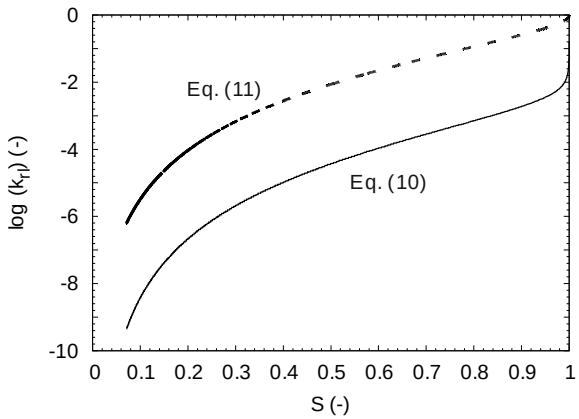

Fig. 3. Comparison of relative permeability to liquid water k_{rl} of CN calculated by Eqs. (10) and (11).

3. Analysis of moisture transport modes

3.1. Boundary conditions

Research results from the literature [18, 19] show that the rate of evaporation at the surface of an almost initially saturated cementitious material is similar to drying of a free surface of liquid water. Hence, a simplification is used to link the drying of a saturated surface with the external relative humidity. For the evaporation from the surface of liquid water, the following equation is used in the literature [19]:

$$w_t = w_l + w_v = \phi S_l E(p_v - p_v^{ext}) \quad (13)$$

where p_v and p_v^{ext} are the internal water vapor pressure near the surface of the specimen and the external water vapor pressure, respectively. E is the emissivity coefficient, which depends on environmental conditions, including wind velocity and temperature. In Eq. (13), ϕS_l stands for the reduction of accessibility due to the presence of a solid phase. By means of a drying experiment of a

free surface of water (at RH = 50 ± 5% and T = 20 ± 1 °C), it was found E = 2.582 × 10^{-8} kg·m^{-2}·s^{-1}·Pa^{-1} (in a case ϕ = 1 and S_l = 1) [14].

3.2. Existence of gas overpressure and underpressure

Substituting the gas flux equation (see Eq. (5)) into the molar balance equations (see Eqs. (2) and (3)), the influence of drying on the gas pressure appears as:

$$\phi(1-S_l)\frac{\partial p_g}{\partial t} = \mathrm{div}\left[p_g \frac{K_g}{\eta_g} k_{rg}(S_l)\,\mathbf{grad}\, p_g\right] + \phi p_g \frac{\partial S_l}{\partial t} + \frac{RT}{M_v}\mu \qquad (14)$$

The individual terms on the right-hand side of Eq. (14) refer to the advective Darcean flow of gas (the first term), the effect of desaturation of the porosity (the second term) and the exchange between liquid water and water vapor (the third term). The first term changes with the gradient of p_g and dissipates the variations of gas pressure. The second term is related to the decrease in S_l and causes a drop in p_g owing to the disappearance of liquid water in the pores. The third term involving the evaporation rate μ can engender an increase in p_g. The vapor pressure is indeed limited by the saturating vapor pressure as the upper bound, which is much lower than the gas overpressure. When the evaporated water vapor is forced to diffuse toward the surrounding air, the diffusion of dry air entries and takes the place of water vapor simultaneously. Consequently, a gas overpressure appears due to the arrival of dry air.

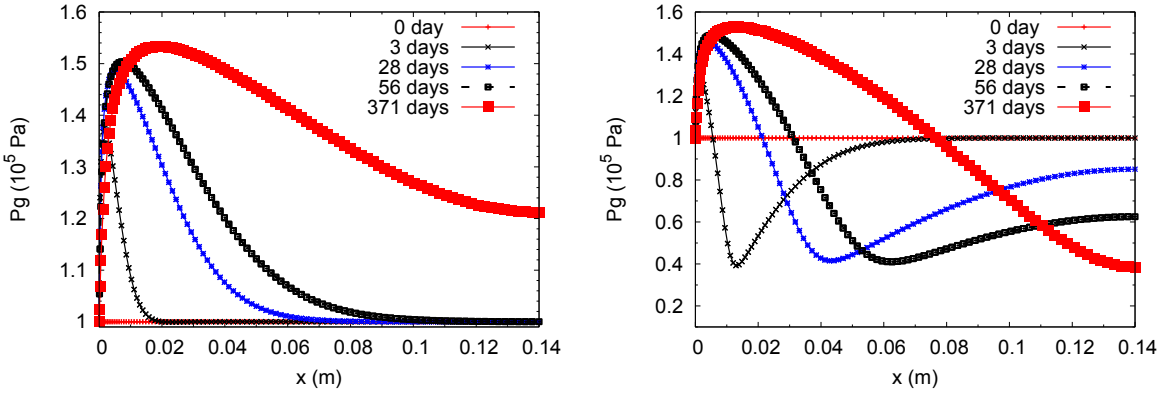

Fig. 4. Profiles of gas pressure during drying of CN for RH_{ext} = 53% and initial S_l^0 = 90% (left) and 99% (right). The profile at 0-day corresponds to the atmospheric pressure.

Simulation results of gas pressure profiles during drying for RH_{ext} = 53% are shown in Fig. 4. Two different initial conditions are considered: S_l^0 = 90 % and 99 %. A significant gas overpressure appears at the border layer of the specimen and the predicted gas pressure can reach up to 1.5 times the initial value of the atmospheric pressure. This is rather unusual because the gas conductivity of porous materials is generally so high that any change of the gas pressure vanishes quasi-instantaneously. Nevertheless, numerical simulations [4] have already shown that the advective Darcean transport of gas (the first term in Eq. (14)) is low for weakly permeable materials such as cementitious materials. Thus, the overpressure phenomena related to liquid water evaporation are not easily dissipated and the role of the third term in Eq. (14) is predominant.

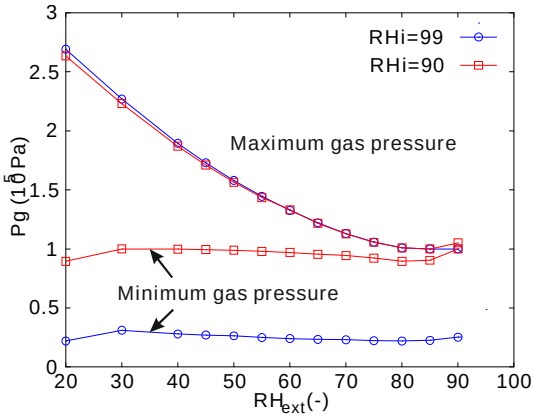

Fig. 5. The maximum and minimum gas pressure during drying of CN for 371 days for various values of RH_{ext} (20% to 90%) and two different initial S_l^0 = 90% (squares) and 99% (circles).

It is worth noting that when the initial condition S_l^0 is 99%, an obvious gas underpressure behaviour can be observed (see Fig. 4). It gradually moves toward the inner part of the specimen, while for a lower initial condition S_l^0=90%, there is no observed gas underpressure. On the one hand, the drying of a material which is initially close to saturation shows significant movements of liquid water due to the strong gradient of capillary pressure. On the other hand, the diffusion coefficient of water vapor is low because of the high water

content according to Eq. (6), so that the diffusion of water vapor is restricted and cannot move to inside the specimen. In this process, the desaturation of the porosity caused by the liquid water flow contributes to decrease the pressure within the material (the second term in Eq. (14)).

Besides, almost the same maximum values of overpressure for two different initial saturations are found in Fig. 4. A series of simulations on various external RH and initial S_l have shown that, for a given material (such as CN), the major factor determining the maximum overpressure during drying is the external RH. For example, the same maximum overpressure variation can be observed for two different initial conditions in Fig. 5, which illustrates the maximum and minimum gas pressures varying with external RH. Another conclusion which can be drawn from simulations in Fig. 5 is that the minimum gas pressure mainly depends on the initial saturation whereas gas underpressure behaviour becomes significant if the initial saturation increases close to saturated state.

3.3. The moisture transport modes

Drying of a porous material is mainly controlled by two modes: (1) the liquid water in the specimen moves to the boundary due to the advective Darcean transport and then evaporates; and (2) the liquid water evaporates to water vapor within the pores which diffuses through the porous network to the surrounding environment. For our simulations, the contribution of water loss in liquid form (time integration of w_l at the boundary) to the total mass loss (time integration of $w_l + w_v$) is plotted in Figs.6 and 7 to identify main modes of moisture transport.

The drying experiments were carried out for CO, CN and CP specimens, which were exposed to a laboratory environment (RH_{ext} = 50 ± 5% at T = 20 ± 1 °C). The following simulations use the same conditions to experiments. Fig. 6 illustrates kinetics of water loss, both liquid water movement and water vapor diffusion during drying a CN specimen (initially S_l^0 = 97%). It clearly shows that the contribution of water vapor increases with the decrease of S_l. That is because liquid water is progressively released from the porous network which enhances the diffusion of water vapor. More precisely, it is observed that at the beginning of drying the mass loss related to liquid water movement plays a key role while the contribution of water vapor increases gradually with time.

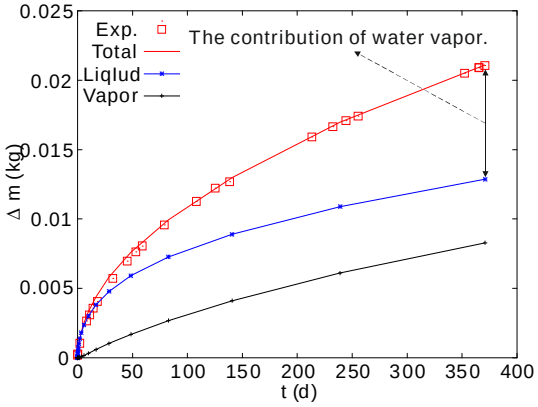

Fig. 6. Mass loss kinetics and contribution of liquid water movement and water vapor diffusion during drying of CN for S_l^0 = 97% and RH_{ext} = 50 ± 5%. The total mass loss is fitted by experimental data (squares) through "inverse analysis" to predict K (see section 2.4.2).

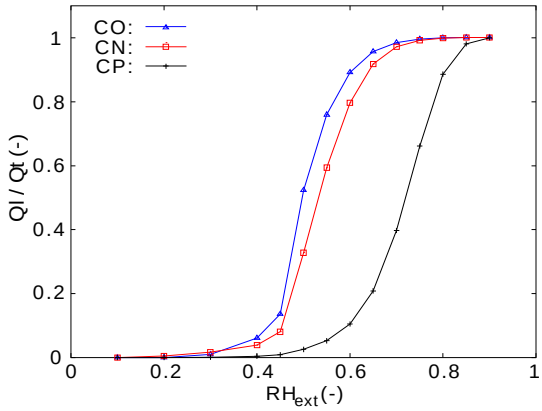

Fig. 7. Comparison of the contribution of water loss in liquid form to the total mass loss during drying of CO, CN and CP for initial S_l^0=90% and various RH_{ext} (10% - 90%).

Moreover, simulations of the contribution of liquid water transport are also carried out for CO, CN and CP for an initial S_l^0= 90% and various RH_{ext} (from 10% to 90%). The numerical results are illustrated in Fig. 6. It is clear that the liquid water contribution on the mass loss during drying depends on the external RH and the kind of material. Several phenomena can be observed in this figure.

(1). For low values of external RH, water vapor diffusion dominates the mass loss (mode (2)), while for high values of external RH, liquid water movement plays the main role (mode (1)). Here, we recall that the mass loss is calculated at the boundary of the specimen, so the analysis is just focused on the surface. The liquid permeability ($k_l = K \cdot k_{rl}$) and gas permeability ($k_g = K \cdot k_{rg}$) are illustrated in Fig. 8. The figure gives that for a given material (such as CN), if the external RH is lower, which also corresponds a lower S_l, the gap between gas permeability and liquid permeability is also larger than

high values of external RH. In addition, for lower values of external S_l, a higher vapor diffusion coefficient can be achieved in Fig. 1. Actually, Eq. (14) reveals that the lower external RH generates less gas pressure variations in the specimen, which is beneficial to water vapor diffusion [4]. So a higher gap between external RH and initial S_l may accelerate both the diffusion and advective Darcean transport of water vapor at the boundary. While the liquid water movement is inactive for low values of external RH due to low liquid water permeability.

(2). For a given external RH, CP always shows the weakest contribution of liquid water, while it is higher for CN and CO. It is natural to link the phenomena with the microstructure (porosity) of the specimen. In the material of larger porosity (such as CP), the gas pressure variations are not significant (see Eq. (14)), so the water vapor can diffuse easier compared with the material of lower porosity. According to Eq. (4), liquid water movement is mainly controlled by the liquid permeability and the gradient of liquid pressure (or the gradient of capillary pressure). The derivation of Eq. (9) shows that the gradient of capillary pressure for CO is always larger than CN and CP. Even though the liquid permeability for CP is a slightly higher as shown in Fig. 8, the gradient of capillary pressure plays a significant role in liquid water movement. Hence, more moisture can be transferred to move to the surface in vapor form and leave the CP specimen than the other two cement pastes.

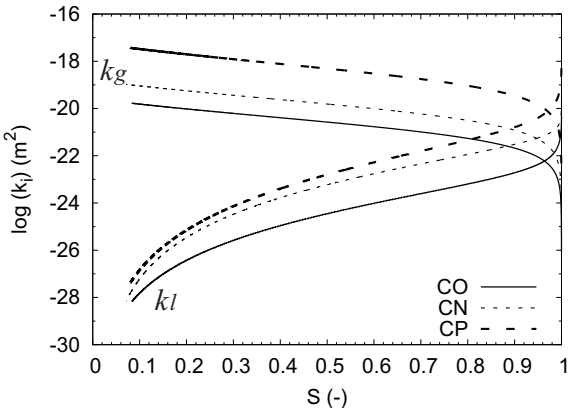

Fig. 8. Comparison of the liquid permeability and gas permeability for CO, CN and CP by the proposed model.

3.4. Comparison with Mainguy's model

Mainguy et al. [4] have developed a model to analyse the drying properties. Two main differences between Mainguy's model and the model proposed in this paper are (1) different choices of parameters a and b for the resistance factor (see Section 2.2, Eq.(6)) and (2) different equations for relative permeabilities (see Section 2.4, Eqs. (10) and (11)).

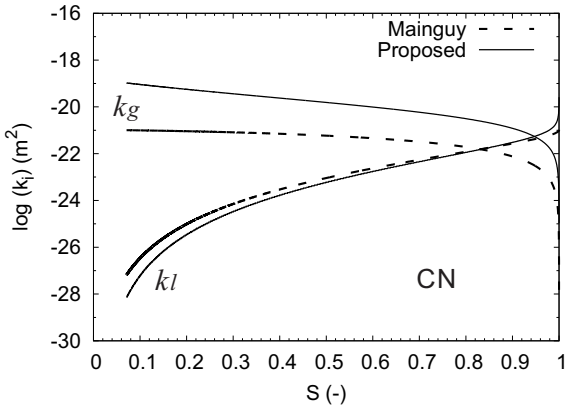

Fig. 9. The comparison of liquid permeability and the gas permeability predicted by Mainguy's model and the proposed model.

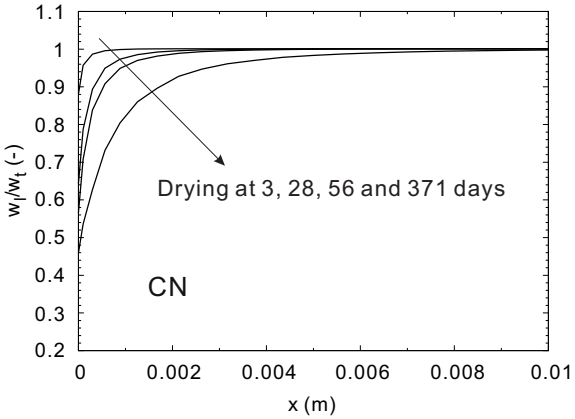

Fig. 10. Ratio of liquid water movement to the total mass flow in the specimen at different ages predicted by the proposed model. Results are from simulations drying of CN for S_l^0 = 90% and RH_{ext} = 50%.

Applying an "inverse analysis" for fitting the intrinsic permeability for both models, we find that it is 10.5×10^{-22} m^2 for CN in Mainguy's model, which is far smaller than the value estimated by the proposed model (16.0×10^{-20} m^2, see Table 3). The liquid permeability (k_l) and the gas permeability (k_g) predicted by Mainguy's model and proposed model are compared in Fig. 9. The gas permeability used in proposed model is higher Mainguy's model in several orders of magnitude. If S_l is smaller than 0.9, Mainguy's model predicts a slightly higher liquid permeability. In fact, the similar results could be achieved for CO and CP. In Fig 1, Mainguy's model always chooses the higher gas diffusion coefficient than the proposed model, either for CO or CN (or CP).

Hence, it is clear that Mainguy's model predicts higher liquid water movement (see Eq. (4)), higher water vapor diffusion while lower advective Darcean transport of water vapor (see Eq. (5)). Simulations by Mainguy's model for CO, initial S_l^0 = 90% and RH_{ext} = 50%, have shown that drying is achieved by the transport of moisture in its liquid form [4]. This conclusion is different from simulation results of the proposed model (see Fig. 7), giving only around 50% contribution of mass loss in liquid form if the external RH is 50%. Drying of CN at the same condition also shows that the liquid water movement in the material decreases with the drying time (see Fig. 10). Besides, because of the advective Darcean transport for gaseous phase (the first term in Eq. (14)), which is able to dissipate the gas pressure variations, is underestimated in Mainguy's model, it predicts a higher gas overpressure reaching to 2 times the atmospheric pressure (see Fig. 11) than gas pressure simulated by the proposed model (see Fig. 4).

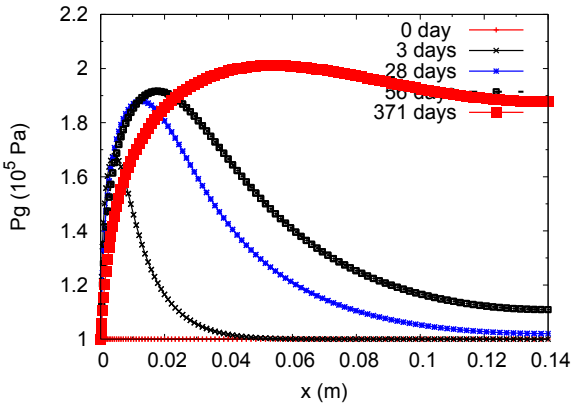

Fig. 11. Profiles of gas pressure during drying of CN performed by Mainguy's model for initial S_l^0 = 90%. The profile at 0-day corresponds to the atmospheric pressure.

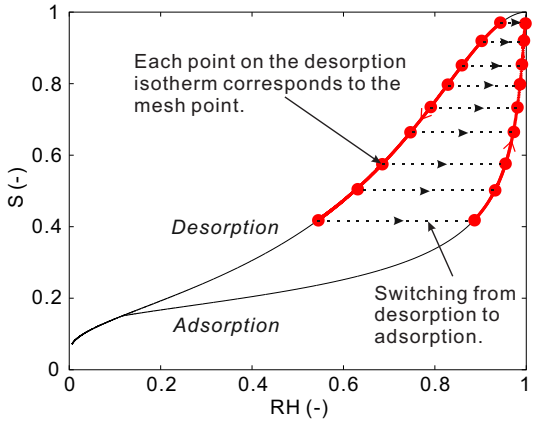

Fig. 12. Schematic figure of switching the desorption isotherm to adsorption isotherm.

4. Modelling moisture transport during drying-wetting cycles

4.1. A simplified concept for modelling of wetting

The simulation of drying and wetting cycles usually needs additional experimental data of scanning curves, which are not easy to be measured. Here, we propose a simplified modelling based on the same isothermal moisture transport model described in Section 2. During drying, the desorption isotherm is used. For wetting, the adsorption isotherm is employed to describe the relationship between RH and S_l. At the end of drying, all points within the specimen are switched directly from desorption isotherm to adsorption isotherm (see Fig. 12).

4.2. Results and discussion

After a drying experiment at external RH = 50 ± 5% for 371 days, CN and CP specimens are exposed to a high level of RH = 97% to provoke wetting. Using the drying kinetics, the intrinsic permeability is obtained by "inverse analysis". It is rarely found the distinguishing of intrinsic permeability during drying and wetting in the literature. As an intrinsic property of the material, we assure that the intrinsic permeability is the same during wetting and drying (see Table 3).

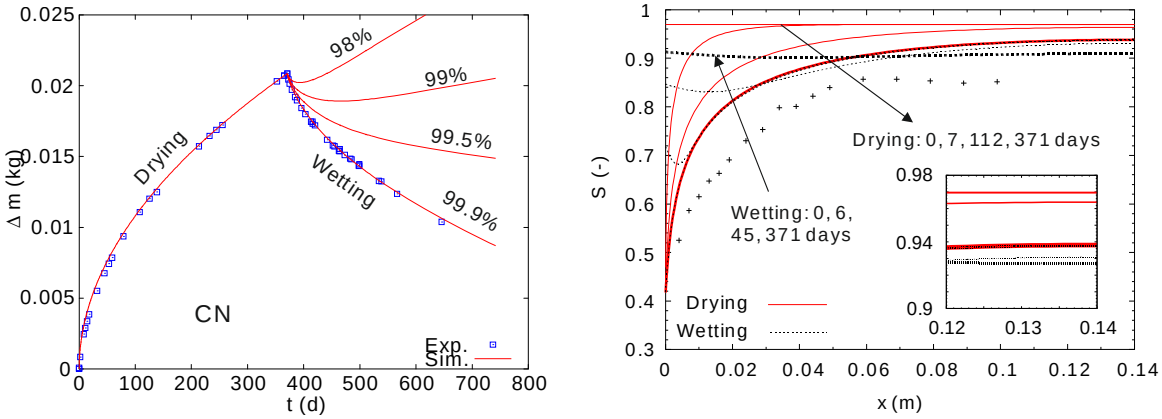

Fig. 13. One drying-wetting cycle simulation results for CN (K= 16.0×10^{-20} m^2). Left: comparison of experimental (symbols) and simulated (lines) mass loss kinetics. Wetting kinetics for different values of external RH are illustrated. Right: profiles of S_l during drying (solid lines) and wetting (dashed lines) at different ages (a zoomed in figure included). The wetting profiles are obtained at RH_{ext} = 99.9%. Symbols are measured data by gamma ray attenuation at the end of drying (371 days).

One drying and wetting cycle simulation is performed for CN and CP using the same duration to the experiment and the results are shown in Figs. 13 and 14, respectively. Simulated wetting kinetics for various external RH (98% - 99.9%) are compared in figures. It can be clearly seen that this simplified concept model is inadequate to the experimental condition (RH = 97%). Only if the external RH is increased to close to the saturated state, very good results for both materials can be observed.

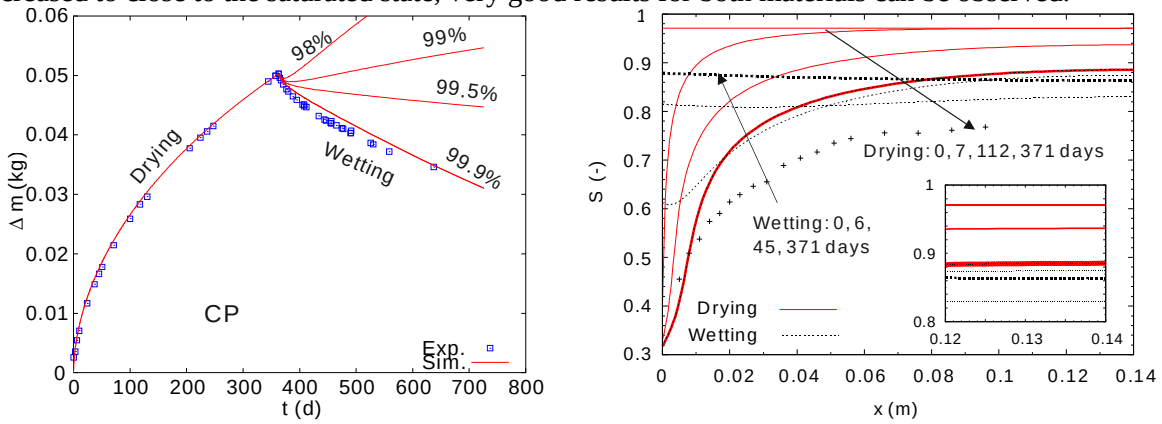

Fig. 14. One drying-wetting cycle simulation results for CP (K= 605.0×10^{-20} m^2). Left: comparison of experimental (symbols) and simulated (lines) mass loss kinetics. Wetting kinetics for different values of external RH are illustrated. Right: profiles of S_l during drying (solid lines) and wetting (dashed lines) at different ages (a zoomed in figure included). The wetting profiles are obtained at RH_{ext} = 99.9%. Symbols are measured data by gamma ray attenuation at the end of drying (371 days).

Comparison of mass loss kinetics shows that if the external RH is lower, such as 98%, the specimen continues to loss mass rather than to wet. A careful analysis reveals that, when the desorption isotherm is switched directly to the adsorption isotherm, the RH inside the specimen is increased improperly. Taking CN as an example, as shown in Fig. 15, according to the adsorption isotherm RH_{ext} = 98% corresponds to S_l^{ext} ≈ 73%. This value is smaller than S_l for most points within the specimen (see the saturation profile at the end of drying in Fig. 13). Thus, at the beginning of wetting, these points, whose saturation is bigger than 73%, will continue to loss mass. Profiles of S_l within the specimen decrease at the beginning of wetting and then rise, as shown in the zoomed in view in Figs. 13 and 14.

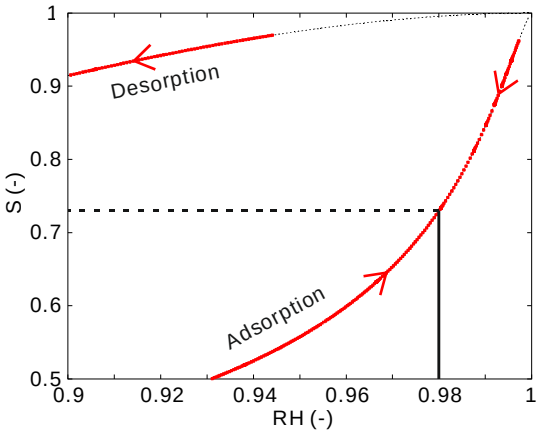

Fig. 15. Partial enlarged drawing of Fig. 12.

If the external RH is increased artificially up to 99.9%, the influence of this issue can be reduced (comparison

of wetting kinetics for different external RH in Fig. 13) and the simulation results are consistent with the experimental data.

5. Conclusion

By means of numerical simulations, this article studies drying of cementitious specimens with a model involving dry air and water vapor as gas phase and pure liquid water phase. Simulation results show that the diffusion of dry air coupled with the movement of water vapor due to evaporation engenders a gas overpressure near the boundary and propagating inside the specimen. Simultaneously, the significant liquid water movement in the inner part of the specimen can cause a gas underpressure. The investigation shows that maximum values of gas pressure are mainly related to external RH, while minimum values are determined by the initial liquid water saturation of the specimen. With regard to the modes of mass loss during drying, they depend on external RH and material microstructure (porosity).

This paper also compares the proposed model with Mainguy's model, which uses different equations for relative permeability and resistance factor. The comparisons point out that Mainguy's model overestimates the contribution of liquid water due to using a slightly higher liquid permeability. On the contrary, it underestimates the advective Darcean transport for the gaseous phase because of the lower gas permeability, so it also predicts a higher gas overpressure than the proposed model.

A simplified concept for the modelling of wetting is proposed in the last part of this paper. Results present that the simplified model is only valid for very high external RH (close to saturated state). It would be welcome to extend the model to suit for different external RHs by using new method to switch the sorption isotherm from desorption to adsorption. That would be our next step research.

Acknowledgements

The research leading to these results has received funding from the European Union Seventh Framework Programme (FP7 / 2007-2013) under grant agreement 264448.

References

[1] Daïan, J. F. "Condensation and isothermal water transfer in cement mortar. Part I.", Transport in Porous Media, 3:563-589, 1988.
[2] Bažant, Z. P. and Kim, J. K. "Consequences of diffusion theory for shrinkage of concrete", Materials and Structures, 24: 323-326, 1991.
[3] Philip, J. R., de Vries D. A. "Moisture movement in porous materials under temperature gradients", Transport Am. Geophysics Union, 38(2):222-232, 1957.
[4] Mainguy, M., Coussy O. and Baroghel-Bouny, V. "Role of air pressure in drying of weakly permeable materials", Journal of Engineering Mechanics, 88:582-592.2001.
[5] Thiéry, M., Belin, P., Baroghel-Bouny, V. and Nguyen, M. D. "Modelling of isothermal drying process in cementitious materials – Analysis of the moisture transfer and proposal of simplified approaches", 3rd International conference on couple THMC, Processes in geo-systems, 571-581, 2008.
[6] Johannesson, B. and Janz, M. "A two-phase moisture transport model accounting for sorption hysteresis in layered porous building constructions", Building and Environment, 44:1285-1294, 2009.
[7] Li, K. and Li, C. "Hydro-ionic transport in concrete near surface under drying-wetting cycles", Mechanics and Physics of Porous Solids (MPPS), 221-240, 2011.
[8] Baroghel-Bouny, V. "Water vapour sorption experiments on hardened cementitious materials. Part I. Essential tool for analysis of hygral behaviour and it relation to pore structure", Cement and Concrete Research, 37:414-437,2007.
[9] Baroghel-Bouny, V. "Water vapour sorption experiments on hardened cementitious materials. Part II. Essential tool for assessment of transport properties and for durability prediction", Cement and Concrete Research, 37:438-454, 2007.
[10] Millington, R. "Gas diffusion in porous media", Science, 130:100-102, 1959.
[11] Papadakis, V., Vayenas, C. and Fardis, M. "Physical and chemical characteristics affecting the durability of concrete", ACI Materials Journal, 8(2):186-196, 1991.
[12] Hassanizadeh, S. M., and W. G. Gray. "Thermodynamic Basis of Capillary Pressure in Porous Media", Water Ressources Research, 29 (10): 3389-3405, 1993.
[13] van Genuchten, M.Th. "A close-form equation for predicting the hydraulic conductivity of unsaturated soils", Soil Science Society of America Journal, 892-898:1980.

[14] Coussy, O., Baroghel-Bouny, V., Dangla, P. and Mainguy, M. “Assessment of the water permeability of concretes from their mass loss during drying (in French)”, in: V. Baroghel-Bouny (Ed.), Transferts dans les bétons et durabilité, Special issue of Revue Française de Génie Civil, vol. 5, Hermès Science Publications, Paris, 269–284, 2001.
[15] Nguyen, M.D. “Modelling the coupling between hydration and drying of cementitious materials after the formwork removal: Study of the degradation transfer properties (in French)”, PhD thesis, ENPC, 2009.
[16] Mualem, Y. “Hysteresis models for prediction of the hydraulic conductivity of unsaturated porous media”, Water Resources Research, 12(6):1248-1254, 1976.
[17] Parker, J. C., Lenhard, R. J., and Kuppusamy, T. “A parametric model for constitutive properties governing multiphase flow in porous media”, Water Resources Research, 23(4):618-624, 1987.
[18] Al-Fadhala, M. and Hover, K-C. “Rapid evaporation from freshly cast concrete and the gulf environment”, Construction and Building Materials, 15:1-7, 2001.
[19] Azenha, M., Maekawa, K., Ishida, T. and Faria, R. “Drying induced moisture losses from mortar to environment. Part I. Experimental research”, Materials and Structure, 40:801-811, 2007.